nature physics

LETTERS

PUBLISHED ONLINE: 30 OCTOBER 2011 | DOI: 10.1038/NPHYS2128

Quantum phase transition to unconventional multi-orbital superfluidity in optical lattices

Parvis Soltan-Panahi†, Dirk-Sören Lühmann†, Julian Struck, Patrick Windpassinger and Klaus Sengstock*

Orbital physics plays a significant role for a vast number of important phenomena in complex condensed-matter systems, including high-temperature superconductivity and unconventional magnetism. In contrast, phenomena in superfluids—in particular in ultracold quantum gases—are typically well described by the lowest orbital and a real order parameter[1]. Here, we report on the observation of a multi-orbital superfluid phase with a complex order parameter in binary spin mixtures. In this unconventional superfluid, the local phase angle of the complex order parameter is continuously twisted between neighbouring lattice sites. The nature of this twisted superfluid quantum phase is an interaction-induced admixture of the *p*-orbital contributions favoured by the graphene-like band structure of the hexagonal optical lattice used in the experiment. We observe a second-order quantum phase transition between the normal superfluid and the twisted superfluid phase, which is accompanied by a symmetry breaking in momentum space. The experimental results are consistent with calculated phase diagrams and reveal fundamentally new aspects of orbital superfluidity in quantum gas mixtures. Our studies might bridge the gap between conventional superfluidity and complex phenomena of orbital physics.

The topological properties of graphene and its remarkable band structure have recently opened a new field in physics[2]. The linear dispersion relation at the Dirac points proves to be a fascinating key aspect of this material, as it gives rise to phenomena such as quasirelativistic particles[3] and an anomalous quantum Hall effect[4,5]. The possibility to realize hexagonal optical lattices[6] enables the emulation of graphene-like physics with ultracold atoms[7–9]. In particular, loading bosonic particles in such lattices renders completely new possibilities such as studying next-nearest-neighbour processes and tunnelling blockades in multicomponent systems[6]. In general, optical lattices have proven to be a versatile tool to simulate Hubbard-like systems and actively drive and monitor quantum phase transitions[10–14]. The important role of higher orbitals has recently been demonstrated for quantum gas mixtures in the strongly correlated regime[15–18]. However, for weakly interacting systems such as superfluids, higher orbitals are generally expected to have only marginal effects. So far, orbital superfluidity has been observed only in excited states with limited lifetimes[19–21].

Here, we demonstrate the realization of a bosonic superfluid ground state where higher-orbital physics plays a crucial role. In conventional superfluids (Fig. 1a), the local phase angle $\Phi(\mathbf{r})$ of the order parameter

$$\varphi(\mathbf{r}) = \sqrt{n(\mathbf{r})}\mathrm{e}^{i\Phi(\mathbf{r})} \qquad (1)$$

is constant (represented by arrows), where $n(\mathbf{r})$ denotes the particle density. Therefore, the order parameter $\varphi(\mathbf{r})$ can be chosen as real. In contrast, the observed twisted superfluid (TSF) ground state reveals a non-trivial complex superfluid order parameter, where the phase factor $\mathrm{e}^{i\Phi(\mathbf{r})}$ is continuously twisted in the complex plane (Fig. 1b). As we shall demonstrate, this unconventional behaviour arises from a strong interaction-induced coupling of *s* and *p* orbitals at zero quasimomentum. This is fundamentally different to previous studies where all atoms are excited to the metastable *p* orbital and condense at finite quasimomentum[19–25]. Most strikingly, even a quantum phase transition between the normal superfluid (NSF) and the TSF phase is directly observed in our experiment. It is driven by the competition between intra- and interspecies interactions in binary mixtures coupling *s* and *p* bands. More precisely, in shallow lattices the intraspecies interaction W_{sp} dominates, whereas the interspecies interaction V_{sp} dominates for intermediate lattice depths, which is further elaborated below. For the experimental realization, we use a 1:1 mixture of ultracold ^{87}Rb atoms in two spin states $|F, m_F\rangle$ of the hyperfine manifold $F = 1, 2$ with Zeeman states m_F (see Methods). The repulsively interacting atoms are confined in a spin-dependent hexagonal optical lattice[6].

As a central aspect, the formation of the twisted superfluid phase originates from both the spin dependence and the specific topology of the hexagonal lattice. The topology leads to a graphene-like band structure with the particular feature that *s* and *p* bands are separated only by the order of the tunnelling energy. In addition, the spin dependence induces an individual sublattice structure for different $|F, m_F\rangle$ states. This leads to an alternating density modulation for $|F, m_F \neq 0\rangle$ spin states (see Fig. 1c). The mutual interaction between different spin states induces a redistribution of both species, leading to an admixture of the *p* orbital. The combination of both topology and state dependence causes a strong coupling of *s* and *p* bands for the case of spin mixtures.

In the following, we first explain how the TSF phase can be identified experimentally and subsequently discuss theoretical phase diagrams as well as experimental results in detail. The NSF phase possesses the expected six-fold rotational symmetry in momentum space. This is observed in experiments through time-of-flight (TOF) imaging for all single-component spin states and is exemplarily shown for $|1, -1\rangle$ in Fig. 2a. In stark contrast, the twisted superfluid phase is accompanied by a symmetry breaking in momentum space, which appears as an alternating pattern in the first-order momentum peaks (Fig. 2b). This reduced three-fold rotational symmetry reflects the occurrence of a twisted complex phase factor $\mathrm{e}^{i\Phi(\mathbf{r})}$, which we observe only for mixtures of two spin states. We observe no significant decay of the alternating pattern for holding times up to 100 ms. This is comparable to

Institut für Laser-Physik, Universität Hamburg, Luruper Chaussee 149, 22761 Hamburg, Germany. †These authors contributed equally to this work.
*e-mail: sengstock@physnet.uni-hamburg.de.

© 2012 Macmillan Publishers Limited. All rights reserved.

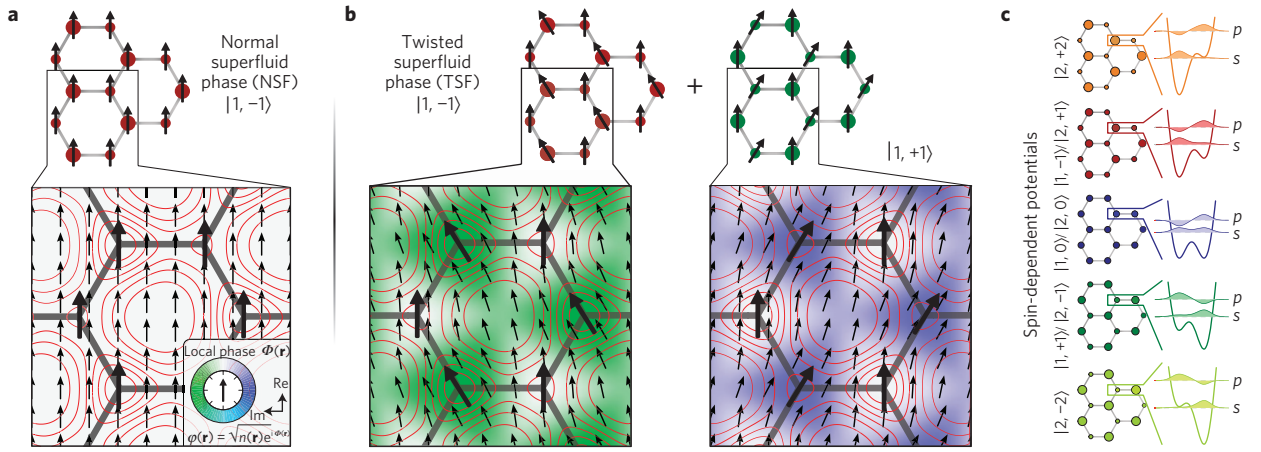

Figure 1 | Normal and twisted superfluid phases. a,**b**, The contour plots depict the superfluid order parameter $\varphi(\mathbf{r}) = \sqrt{n(\mathbf{r})}e^{i\Phi(\mathbf{r})}$ (red lines) in the hexagonal lattice. The arrows and colour coding represent the local phase angles $\Phi(\mathbf{r})$. **a**, Normal superfluid: single-component spin systems exhibit a real superfluid order parameter with constant local phases. **b**, Twisted superfluid: in binary spin mixtures, the local phases $\Phi(\mathbf{r})$ vary continuously between the sites of the hexagonal lattice, leading to a complex superfluid order parameter for both components. This twisted phase is caused by a complex admixture of the *p* band. **c**, The spin-dependent lattice causes a density modulation in dependence on the spin state $|F, m_F\rangle$. The *s*- and *p*-orbital wavefunctions as well as the spin-dependent potentials are shown as a one-dimensional cut along two adjacent lattice sites.

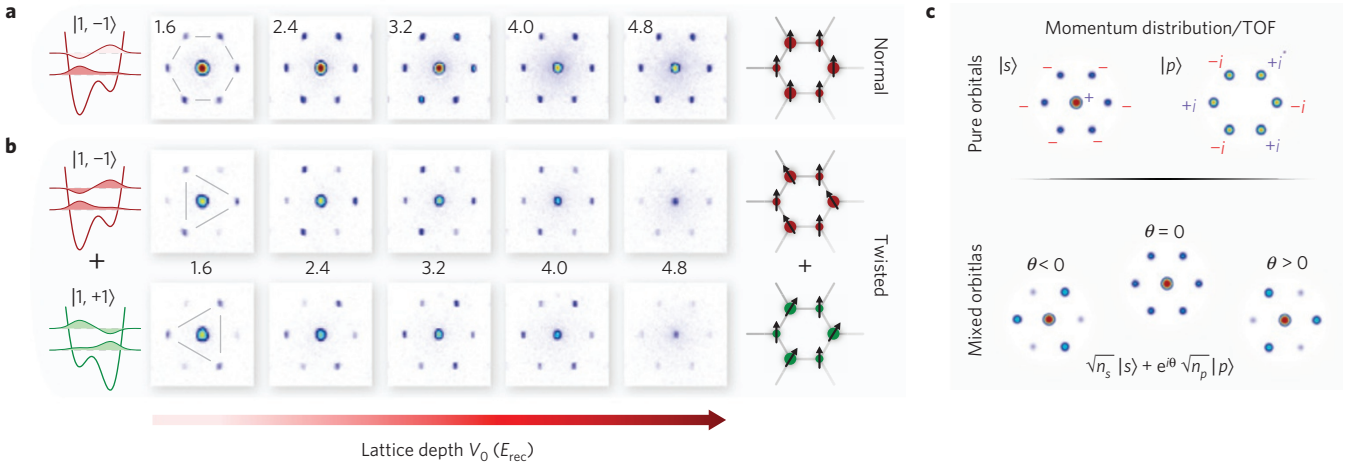

Figure 2 | Symmetry breaking in momentum space. a, The normal superfluid phase shows a six-fold rotational symmetry due to the lattice geometry. Averaged TOF images are shown for different lattice depths (indicated in the images). **b**, For certain binary mixtures, an interaction-induced reduced three-fold rotational symmetry is clearly observed for both constituents being separated by a Stern–Gerlach field (shown is a 1:1 mixture of $|1,-1\rangle$ and $|1,+1\rangle$ atoms). The triangular pattern is opposite for the two constituents. The six-fold rotational symmetry is restored for large lattice depths. **c**, Calculated TOF images reflecting the momentum distributions for *s*- and *p*-orbital wavefunctions for $|F, m_F = 0\rangle$, where the *p*-orbital wavefunction in momentum space is complex and has an alternating sign in its first-order peaks. A complex superposition of the two orbitals leads to the observed triangular TOF pattern for the TSF phase even for small admixtures of the *p* orbital, whereas for real superpositions the six-fold rotational symmetry is preserved (shown for *p*-band admixtures of $n_p = 1 - n_s = 0.05$ and $\theta = 0, \pm\pi/2$).

the lifetime of the normal superfluid, reflecting the ground-state nature of the twisted superfluid phase. Figure 2b shows the results for a 1:1 mixture of $|1,-1\rangle$ and $|1,+1\rangle$ atoms, where the spin states are separated in the experiment by a Stern–Gerlach field. The occurrence of the twisted superfluid phase is clearly visible for very small lattice depths. Here, both components show a complementary momentum distribution reflecting the opposite phase twist as indicated in Fig. 1b. For increasing lattice depths, the transition to the normal superfluid phase is observed by the restoration of the six-fold rotational symmetry (Fig. 2b). Finally, the overall interference contrast vanishes as the system approaches the Mott insulator phase, where the atoms localize on individual lattice sites.

Remarkably, the clear signature of the TSF phase persists even for *p*-band admixtures as small as a few per cent, which is a typical value in our experiment. This relies on the fact that the first-order momentum peaks of the *p* orbital are much stronger than those of the *s* orbital, leading to a strong amplification of the *p*-band contributions, which can be clearly identified in the TOF images (see Fig. 2c). The observed alternating pattern for the twisted superfluid is caused by the quantum interference of *s*- and *p*-band contributions at zero quasimomentum (see equation (4)), which enables an extremely sensitive probing of the local phase properties through TOF. Note that the interference requires that *s*- and *p*-orbital contributions occupy the same quasimomentum state (here $\mathbf{q} = 0$).

The connection between the hybridization of *s* and *p* orbitals and the transition to the TSF phase can be explained as follows. In general, a superposition between *s* orbital $|s\rangle$ and *p* orbital $|p\rangle$ can be written as

$$|\varphi\rangle/\sqrt{N} = \sqrt{n_s}|s\rangle + e^{i\theta}\sqrt{n_p}|p\rangle \qquad (2)$$

© 2012 Macmillan Publishers Limited. All rights reserved.

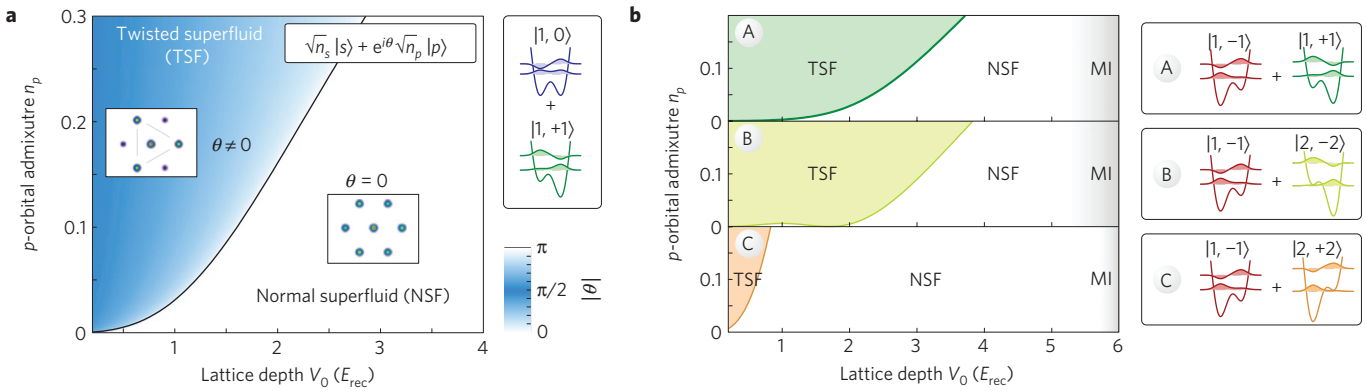

Figure 3 | Quantum phase transition to a twisted superfluid phase. a, Zero-temperature phase diagram for the $|1,0\rangle$ state in an equal admixture with the $|1,+1\rangle$ state. The diagram is parameterized by the relative occupation of the p orbital $n_p = 1 - n_s$ and the hexagonal lattice depth V_0. The white area defines the NSF and the blue area the TSF, where the colour encoding represents the value of the order parameter θ. **b**, Phase diagram of $|1,-1\rangle$ in an equal admixture with $|1,+1\rangle$ (A), $|2,-2\rangle$ (B) and $|2,+2\rangle$ (C). For a lattice depth of $V_0 = 5$–$6\,E_{rec}$, the system undergoes the transition to a Mott insulator (MI), where the entrance points depend on the particular spin mixture[6].

where the coefficients n_s and n_p denote the fraction of atoms in the s and the p orbital, respectively, and N the total number of particles. The global phase angle θ between the two orbitals is crucial for the formation of the twisted superfluid. It takes the value which minimizes the energy of the system and can lead to two different physical situations: For $\theta = 0$ (or π), the system is in the normal superfluid phase, where no interference takes place and the alternating momentum pattern vanishes (Fig. 2c). In contrast, $\theta \neq 0$ causes a destructive interference of the first-order peaks, thereby revealing the twist of the local phases $\Phi(\mathbf{r})$. Thus, the global phase angle θ takes the important role of an order parameter describing the phase transition between NSF and TSF, where the TSF phase is defined by a non-zero value of θ.

We explore this phase transition theoretically using a multiband mean-field approach (see Methods), which leads to the phase diagrams presented in Fig. 3. The phase diagrams show the results for different binary spin mixtures. In agreement with the experimental results, the twisted superfluid emerges only in shallow lattices. It is important to mention that, in our hexagonal optical lattice configuration, different spin states preferably occupy different sublattices and therefore the interplay of intra- and interspecies interaction strongly depends on the spin mixture considered. In particular, the phase diagrams in Fig. 3b demonstrate that the TSF phase area is drastically reduced for spin mixtures predominantly occupying the same sublattice (mixture C) in comparison with spin mixtures where each component occupies a different sublattice (mixtures A and B). In addition, the occurrence of the TSF phase depends on the admixture of the p-band orbital, where n_p vanishes at zero lattice depth and is expected to reach a few per cent for intermediate lattice depths under experimental conditions. This also explains the absence of the TSF phase for single-component samples (Fig. 2a) where the population of the p orbital is negligible.

In the following, we experimentally investigate the phase diagrams above. As an experimental indicator characterizing the NSF and TSF phase, we define a triangular interference contrast $I_\triangle$, which is illustrated in Fig. 4. It serves as a measure of the order parameter θ of the NSF–TSF transition, where $I_\triangle \neq 0$ corresponds to the TSF phase. For spin mixture A, the TSF phase is clearly resolved for $V_0 < 4\,E_{rec}$ (Fig. 4a), where E_{rec} is the recoil energy. As expected for symmetry reasons, both components exhibit the same triangular contrast $|I_\triangle|$. In the limit of zero lattice depth, the admixture n_p is negligible, which leads to a vanishing $I_\triangle$. As n_p increases with the lattice depth and $I_\triangle$ vanishes at the phase boundary, a maximum can be observed in the triangular interference contrast. In accordance with the phase diagrams presented in Fig. 3, mixture

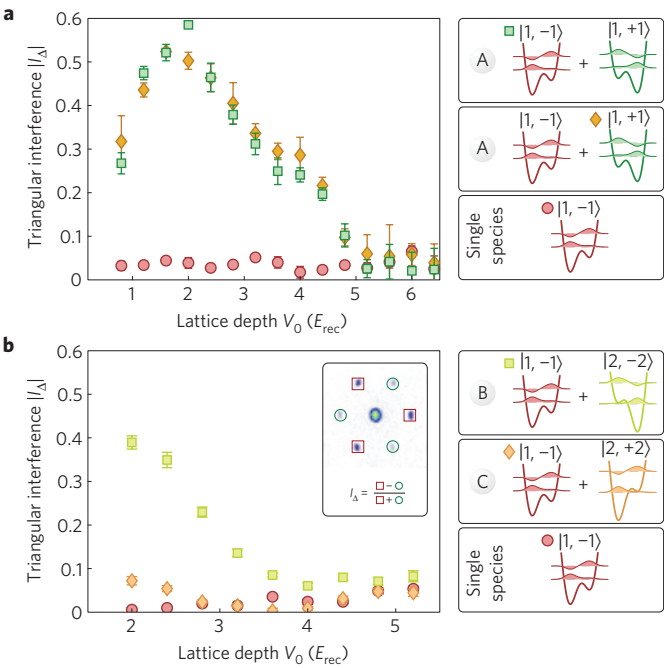

Figure 4 | Observation of the NSF–TSF quantum phase transition. **a**,**b**, Absolute value of the triangular interference contrast $I_\triangle$ (see inset) as a function of the lattice depth V_0 for spin mixture A (**a**) and spin mixtures B and C (**b**). The TSF phase is identified by a non-zero value of $I_\triangle$, whereas $I_\triangle$ vanishes in the NSF phase. The error bars indicate the standard deviation of the mean.

B exhibits a similar behaviour to mixture A, where in both cases different sublattices are occupied by the constituents (Fig. 4b). The substantial difference of the predicted TSF phase areas for mixtures B and C is also clearly revealed in our experiment.

To gain further insight into the underlying processes of the NSF–TSF transition, we turn back to its theoretical description. The observed quantum phase transition is entirely driven by the competition between intra- and interspecies interactions and can thus occur at zero temperatures. We apply mean-field theory, where we restrict our analysis to an effective two-mode Hamiltonian[25] (see Methods). For the superfluid order parameter, we consider s- and p-band contributions described by equation (2), where the order parameter of the transition θ is the relative phase angle

© 2012 Macmillan Publishers Limited. All rights reserved.

between the two orbitals. In the calculation, higher bands and non-zero-quasimomentum states can be ignored to first order.

For simplicity, we discuss here a mixture of $|1,0\rangle$ with $|1,-1\rangle$ atoms (see Fig. 3a). In this case, the symmetry of s- and p-band wavefunctions for $|1,0\rangle$ leads to only two competing θ-dependent terms in the energy functional, namely, the interspecies interaction $v_{sp}(\theta) = 2N^2 V_{sp}\sqrt{n_s n_p}\cos(\theta)$ and the intraspecies interaction $w_{sp}(\theta) = 2N^2 W_{sp}\, n_s n_p \cos(2\theta)$. Here, N is the number of particles in each component; V_{sp} and W_{sp} are integrals of s- and p-orbital wavefunctions with $V_{sp} < 0$ and $W_{sp} > 0$ (see Methods). Physically, v_{sp} describes a collision of two particles with different spin states, where one particle is promoted from the s to the p band, whereas the intraspecies interaction w_{sp} promotes a pair of particles of the same species from the s to the p orbital. For sufficiently small p-band admixtures n_p, the interspecies interaction v_{sp} dominates and therefore $\theta = 0$ minimizes the energy, which corresponds to a normal superfluid. However, for a critical value of n_p the energy functional $v_{sp}(\theta) + w_{sp}(\theta)$ no longer exhibits a minimum at $\theta = 0$. As a central result, this defines the phase boundary n_p^{crit} of the NSF–TSF transition, which is given for the considered case by

$$n_p^{\mathrm{crit}} = \frac{1}{2} - \sqrt{\frac{1}{4} - \left(\frac{V_{sp}}{4W_{sp}}\right)^2} \tag{3}$$

The phase transition is of second order as the second derivative of the energy functional is discontinuous at this boundary. In the applied theory, the Hamiltonian is invariant under the transformation $\theta \to -\theta$ causing a twofold degenerate ground state in the twisted phase. This corresponds to the two possible orientations of the triangular pattern with opposite signs of $I_\triangle$ (see Fig. 2b,c). However, in the experiment always the same one of the two ground states is observed. Further studies are necessary to investigate this non-spontaneous symmetry breaking.

Our study of a new type of complex superfluid phase paves the way for further investigations of the interplay between orbital physics and strong correlations. In particular, a possible competition between the twisted superfluid and the strongly correlated Mott insulator phase can be realized by increasing the interactions, for example by means of Feshbach resonances. Moreover, further insight into the roles of intra- and interspecies interactions can be gained using binary mixtures consisting of two different atomic states, where the two interactions differ considerably from each other. In addition, dynamically driven phase transitions may be observable in our systems by preparing a dynamical superposition of s and p orbitals for one of the two spin components through microwave coupling.

Methods

Creation of spin-dependent hexagonal lattices. The spin-dependent hexagonal lattice is realized by intersection of three coplanar laser beams under an angle of 120°. The laser beams are derived from a Ti:sapphire laser operated at a wavelength $\lambda_L = 830$ nm (red detuned), where each beam is linearly polarized within the plane of intersection. Orthogonal to the plane, we apply a retro-reflected one-dimensional lattice at $V_{1D} = 8.8\, E_{rec}$ operated at the same wavelength (for details see ref. 6). The recoil energy E_{rec} is defined as $E_{rec} = \hbar^2 k_L^2/2m$ with the wavevector of the laser $k_L = 2\pi/\lambda_L$ and the mass m of an ^{87}Rb atom.

Preparation and detection schemes for spin mixtures. We start with a Bose–Einstein condensate of typically several 10^5 atoms in the stretched state $|1,-1\rangle$, which is confined in a nearly isotropic crossed dipole trap with a trap frequency $\omega \approx 2\pi \times 90$ Hz. For these experimental parameters we expect a maximum filling factor of approximately four to six particles per lattice unit cell, which decreases towards the edge of the system owing to the inhomogeneous trapping potential. The preparation of the different pure and mixed spin states is carried out with the aid of radiofrequency and/or microwave sweeps. After the state preparation we apply a homogeneous magnetic field of 1.1 G to suppress spin dynamics[26] and ramp up the optical lattice within 55 ms using an exponential ramp. Within the ramping time the coherence between different spin states is lost. To separate different spin components during 27 ms TOF, a Stern–Gerlach gradient field is applied before absorption imaging. The density distribution after TOF ρ_{TOF} reflects the momentum distribution in the lattice and can be calculated using the Fourier transform of Bloch wavefunctions $\tilde{\varphi}_{s,p}$

$$\rho_{\mathrm{TOF}}(\mathbf{r}) \propto n_s|\tilde{\varphi}_s(\mathbf{k})|^2 + n_p|\tilde{\varphi}_p(\mathbf{k})|^2 + 2\sqrt{n_s n_p}\,\mathrm{Re}\left(\tilde{\varphi}_s^*(\mathbf{k})\tilde{\varphi}_p(\mathbf{k})\mathrm{e}^{i\theta}\right) \tag{4}$$

with $\mathbf{k} = m\mathbf{r}/\hbar t$. Whereas for $\theta = 0$ or π the third term vanishes, it causes an interference effect for other phase angles θ (for example for $|F, m_F = 0\rangle$ as shown in Fig. 2c the function $\tilde{\varphi}_s$ is real and $\tilde{\varphi}_p$ is imaginary). The simulated TOF images in Fig. 2c show the time evolution of the ensemble taking the finite trap size into account.

To verify independently the emerging interference pattern for different values of θ, we carry out a microwave excitation of the spin state $|2,-2\rangle$ to $|1,-1\rangle$. In this way we create a superposition of s and p orbitals in the $|1,-1\rangle$ state, which evolves in time t as $\sqrt{n_s}|s\rangle + \mathrm{e}^{-i\Delta E_{sp}t/\hbar}\sqrt{n_p}|p\rangle$, where the oscillation frequency of the triangular interference contrast $I_\triangle$ matches the energy difference of s and p bands ΔE_{sp}. The observed features show the same pattern as shown in Fig. 2 when replacing θ by the time-dependent expression $\theta \to -\Delta E_{sp}t/\hbar$.

Theoretical model. To first order, N particles of the spin species σ experience the interaction with the non-interacting density $M|\phi_{\sigma'}(\mathbf{r})|^2$ of the other species σ' with M atoms. Thus, we can write the effective Hamiltonian for the spin state σ as

$$\hat{H}_\sigma = \int \mathrm{d}^3 r\, \hat{\psi}_\sigma^\dagger(\mathbf{r})\left[H_0 + g_{\sigma\sigma'}M|\phi_{\sigma'}(\mathbf{r})|^2 + \frac{g_{\sigma\sigma}}{2}\hat{\psi}_\sigma^\dagger(\mathbf{r})\hat{\psi}_\sigma(\mathbf{r})\right]\hat{\psi}_\sigma(\mathbf{r}) \tag{5}$$

where $H_0 = (\mathbf{p}^2/2m) + V(\mathbf{r})$ is the operator for kinetic and potential energy and $\hat{\psi}_\sigma$ is the bosonic field operator. The interaction strength between two spin states $\sigma = |F, m_F\rangle$ and $\sigma' = |F', m_{F'}\rangle$ is labelled by $g_{\sigma\sigma'} = 4\pi\hbar^2 a_{\sigma\sigma'}/m$ with an s-wave scattering length $a_{\sigma\sigma'} \approx 100a_0$ (a_0 is the Bohr radius). For shallow lattices, we assume that only s- and p-band Bloch functions $\varphi_{s,p}$ with quasimomentum $\mathbf{q} = 0$ contribute. For a large total number of particles and weak interactions, we apply mean-field theory and expand the field operators according to equation (2)

$$\hat{\psi}_\sigma(\mathbf{r})/\sqrt{N} \to \sqrt{n_s}\varphi_s(\mathbf{r}) + \mathrm{e}^{i\theta}\sqrt{n_p}\varphi_p(\mathbf{r}) \tag{6}$$

where $\varphi_{s,p}$ are real functions. The energy functional can be divided into a θ-independent and a θ-dependent part, where the latter is given by $H_\theta(n_p, \theta) = v_{sp} + w_{sp} + x_{sp}$ with

$$\begin{aligned} v_{sp} &= 2MNV_{sp}\sqrt{n_s n_p}\cos(\theta) \\ w_{sp} &= 2N^2 W_{sp}\, n_s n_p \cos(2\theta) \\ x_{sp} &= 4N^2\left(X_s n_s + X_p n_p\right)\sqrt{n_s n_p}\cos(\theta) \end{aligned} \tag{7}$$

These terms depend on the interspecies integral $V_{sp} = g_{\sigma\sigma'}\int \mathrm{d}^3 r|\phi_{\sigma'}|^2\varphi_s^*\varphi_p$ And the intraspecies integrals $W_{sp} = (g_{\sigma\sigma}/2)\int \mathrm{d}^3 r\varphi_s^{*2}\varphi_p^2$, $X_s = (g_{\sigma\sigma}/2)\int \mathrm{d}^3 r|\varphi_s|^2\varphi_s^*\varphi_p$ and $X_p = (g_{\sigma\sigma}/2)\int \mathrm{d}^3 r|\varphi_p|^2\varphi_s^*\varphi_p$, where the latter two vanish for symmetric spin states $|F, m_F = 0\rangle$ owing to parity. Without loss of generality, we choose the arbitrary sign of φ_p such that v_{sp} exhibits a minimum for $\theta = 0$ corresponding to $V_{sp} < 0$. The phase boundary of the phase transition between normal and twisted superfluid phases is defined by

$$2W_{sp}\sqrt{n_p(1-n_p)} = \left|\frac{M}{2N}V_{sp} + X_s(1-n_p) + X_p n_p\right| \tag{8}$$

When approaching the Mott insulator transition, higher-quasimomentum states become occupied and the two-mode description presented here is no longer fully valid. This could explain quantitative deviations between theory and experiment.

Received 15 April 2011; accepted 23 September 2011; published online 30 October 2011; corrected online 15 November 2011

References

1. Pitaevskii, L. P. & Stringari, S. *Bose–Einstein Condensation* (Oxford Univ. Press, 2003).
2. Geim, A. K. & Novoselov, K. S. The rise of graphene. *Nature Mater.* **6,** 183–191 (2007).
3. Du, X., Skachko, I., Duerr, F., Luican, A. & Andrei, E. Y. Fractional quantum Hall effect and insulating phase of Dirac electrons in graphene. *Nature* **462,** 192–195 (2009).
4. Novoselov, K. S. *et al.* Two-dimensional gas of massless Dirac fermions in graphene. *Nature* **438,** 197–200 (2005).
5. Zhang, Y., Tan, J. W., Stormer, H. L. & Kim, P. Experimental observation of the quantum Hall effect and Berry's phase in graphene. *Nature* **438,** 201–204 (2005).
6. Soltan-Panahi, P. *et al.* Multi-component quantum gases in spin-dependent hexagonal lattices. *Nature Phys.* **7,** 434–440 (2011).

© 2012 Macmillan Publishers Limited. All rights reserved.

7. Zhu, A-L., Wang, B. & Duan, L-M. Simulation and detection of Dirac fermions with cold atoms in an optical lattice. *Phys. Rev. Lett.* **98,** 260402 (2007).
8. Wu, C. & Das Sarma, S. $p_{x,y}$-orbital counterpart of graphene: Cold atoms in the honeycomb optical lattice. *Phys. Rev. B* **77,** 235107 (2008).
9. Lee, K. L., Grémaud, B., Han, R., Englert, B-G. & Miniatura, C. Ultracold fermions in a graphene-type optical lattice. *Phys. Rev. A* **80,** 043411 (2009).
10. Greiner, M., Mandel, O., Esslinger, T., Hänsch, T. W. & Bloch, I. Quantum phase transition from a superfluid to a Mott insulator in a gas of ultracold atoms. *Nature* **415,** 39–44 (2002).
11. Jördens, R., Strohmaier, N., Günter, K., Moritz, H. & Esslinger, T. A Mott insulator of fermionic atoms in an optical lattice. *Nature* **455,** 204–207 (2008).
12. Schneider, U. *et al.* Metallic and insulating phases of repulsively interacting fermions in a 3D optical lattice. *Science* **322,** 1520–1525 (2008).
13. Struck, J. *et al.* Quantum simulation of frustrated magnetism in triangular optical lattices. *Science* **333,** 996–999 (2011).
14. Bloch, I., Dalibard, J. & Zwerger, W. Many-body physics with ultracold gases. *Rev. Mod. Phys.* **80,** 885–964 (2008).
15. Will, S. *et al.* Time-resolved observation of coherent multi-body interactions in quantum phase revivals. *Nature* **465,** 197–201 (2010).
16. Best, T. *et al.* Role of interactions in ^{87}Rb–^{40}K Bose–Fermi mixtures in a 3D optical lattice. *Phys. Rev. Lett.* **102,** 030408 (2009).
17. Lühmann, D-S., Bongs, K., Sengstock, K. & Pfannkuche, D. Self-trapping of bosons and fermions in optical lattices. *Phys. Rev. Lett.* **101,** 050402 (2008).
18. Lutchyn, R. M., Tewari, S. & Das Sarma, S. Loss of superfluidity by fermions in the boson Hubbard model on an optical lattice. *Phys. Rev. A* **79,** 011606 (2009).
19. Müller, T., Fölling, S., Widera, A. & Bloch, I. State preparation and dynamics of ultracold atoms in higher lattice orbitals. *Phys. Rev. Lett.* **99,** 200405 (2007).
20. Wirth, G., Ölschläger, M. & Hemmerich, A. Evidence for orbital superfluidity in the *P*-band of a bipartite optical square lattice. *Nature Phys.* **7,** 147–153 (2011).
21. Ölschläger, M., Wirth, G. & Hemmerich, A. Unconventional superfluid order in the *F* band of a bipartite optical square lattice. *Phys. Rev. Lett.* **106,** 015302 (2011).
22. Isacsson, A. & Girvin, S. M. Multiflavor bosonic Hubbard models in the first excited Bloch band of an optical lattice. *Phys. Rev. A* **72,** 053604 (2005).
23. Wu, C., Liu, W. V., Moore, J. & Das Sarma, S. State preparation and dynamics of ultracold atoms in higher lattice orbitals. *Phys. Rev. Lett.* **97,** 190406 (2006).
24. Liu, W. V. & Wu, C. Atomic matter of nonzero-momentum Bose–Einstein condensation and orbital current order. *Phys. Rev. A* **74,** 013607 (2006).
25. Zhou, Q., Porto, J. V. & Das Sarma, S. Condensates induced by interband coupling in a double-well lattice. Inter-band coupling induced novel condensates in a double-well lattice. *Phys. Rev. B* **83,** 195106 (2011).
26. Schmaljohann, H. *et al.* Dynamics of $F = 2$ spinor Bose–Einstein condensates. *Phys. Rev. Lett.* **92,** 040402 (2004).

Acknowledgements

The work has been funded by Deutsche Forschungsgemeinschaft grants FOR 801 and GRK 1355 as well as by the Landesexzellenzinitiative Hamburg, which is supported by the Joachim Herz Stiftung.

Author contributions

The experimental work and data analysis were done by P.S-P., J.S., D-S.L., P.W. and K.S. D-S.L. and P.S-P. carried out the theoretical calculations. P.S-P. and D-S.L. wrote the manuscript with substantial contributions by all authors.

Additional information

The authors declare no competing financial interests. Reprints and permissions information is available online at http://www.nature.com/reprints. Correspondence and requests for materials should be addressed to K.S.

© 2012 Macmillan Publishers Limited. All rights reserved.

ERRATUM

Quantum phase transition to unconventional multi-orbital superfluidity in optical lattices

Parvis Soltan-Panahi, Dirk-Sören Lühmann, Julian Struck, Patrick Windpassinger and Klaus Sengstock

Nature Physics http://dx.doi.org/10.1038/nphys2128 (2011); published online 30 October 2011; corrected online 15 November 2011.

In the version of this Letter originally published online, the square-root signs in the formula in Fig. 3a were displayed incorrectly. This has been corrected in all versions of the Letter.

© 2012 Macmillan Publishers Limited. All rights reserved.